JOURNAL OF GEOPHYSICAL RESEARCH, VOL. 99, NO. B8, PAGES 15,529–15,537, AUGUST 10, 1994

Shock wave profile study of tuff from the Nevada Test Site

Dave Erskine, W. J. Nellis, and S. T. Weir
Lawrence Livermore National Laboratory, Livermore, California

Abstract. Shock wave equation of state and release behavior of tuff from the Nevada Test Site were measured in the range 8 to 107 GPa by recording shock wave profiles produced by impact of projectiles accelerated by a two-stage light-gas gun. Shock wave profiles were measured with a fast optical interferometer. Hugoniot, sound speed, and effective Gruneisen parameter data were determined from the profiles. The specimen geometry allows direct observation of the shape of the leading edge of the shock, in which complex compressive dynamics caused by pore crushing or phase transitions can manifest themselves. The tuff specimens were tested in both a water-saturated and semidry state. Hydration of the rock increases both the shock and sound speeds for a given compression. The U_s-U_p relation for our water-saturated tuff is slightly nonlinear and can be approximated as U_s=2.00 + 1.42 U_p for 0<U_p<6 km/s, and U_s=2.29+1.29U_p for 0<U_p<3 km/s. For semidry tuff at pressures less than 18 GPa, U_s=1.70+1.28U_p.

Introduction

Tuff is the major type of rock in which nuclear devices have been tested at the Nevada Test Site (NTS). Knowledge of shock wave propagation behavior in tuff is important for determining the yield of an underground nuclear explosion and for treaty verification. One method to determine the yield, the CORRTEX method, is to measure the time history of the expansion of the shock in the Earth close to a nuclear device and to determine by calculations the energy yield which would produce such a time history. For this application an accurate model of both the shock compressive and release behaviors of tuff is required. The shock compression curve is the Hugoniot. Knowledge of release behavior is necessary because the release wave causes the attenuation of the strength of the leading shock wave as it propagates from the source. The associated shock propagation velocity is also attenuated, thus affecting the time history of the expanding shock in the surrounding rock.

Tuff is a type of volcanic ash which has been partially consolidated by the pressure of the overburden. It is a heterogeneous soft mineral with firm grains (0.5-5 mm) embedded in more loosely bound ash. This heterogeneity combined with tuff's porosity makes its shock behavior difficult to model compared to a hard rock such as granite. In addition to small-scale heterogeneity, the earth at NTS consists of many kinds of tuff having significant variation with elevation in degree of friability, density, grain size distribution, porosity, and water content. This will produce a concomitant variability in the shock behavior, especially at relatively low pressures, where mechanical properties are important. At relatively high pressures the shock results tend to converge for various tuffs. Because of uncertainties at low to moderate shock pressures, determining the nuclear yield has at least two important dimensions: understanding the shock response of a given tuff versus shock pressure and understanding how this response varies with the kind of tuff. Unfortunately, few previous shock wave profile studies have been performed on tuff [*Furnish*, 1990, 1992]. Discussions of the general geology and geophysics of NTS have been published previously [*Howard*, 1985; *Taylor*, 1983]. Descriptions of the calculational modeling of this phenomena have also been published [*Glenn*, 1993].

Recently we studied the shock behavior of the tuff surrounding the Bristol event (November 1991). Samples of tuff were removed from the wall of the emplacement hole at various elevations and brought back to our laboratory for dynamic testing. The tuff's hydration, friability, and grain size varied significantly with elevation on a 3-m scale. Since a detailed investigation of the shock properties of only one such material could be performed, competent tuff from one elevation was selected to be characterized in detail.

The water content of tuff is an important parameter which varies significantly with elevation. In situ hydration can be difficult to preserve as the sample is machined into a form suitable for shock experiments. For this reason we tested tuff from this same batch in both the dry and rehydrated states to learn what effect hydration has on the shock behavior.

The shock wave profiles were measured using a fast optical interferometer called a VISAR (velocity interferometer system for any reflector) that records the continuous motion of the sample undergoing shock compression and release [*Hemsing*, 1979]. The advantage of this diagnostic is that it measures both the structure of the shock wave as well as the shock transit time, and thus the shock speed, across the sample. Methods which measure only the shock transit time are insensitive to the additional information contained in the wave profile. Phase transformations and pore crushing phenomena are two examples of processes which manifest themselves in the wave-profile structure. Shock wave profiles have been employed, for example, to observe the graphite to diamond phase transition in graphite [*Erskine and Nellis*, 1991, 1992] and the α–quartz to stishovite phase transition [*Swegle*, 1990]. The unloading or release behavior manifested in the wave profiles has been used extensively to study phase transitions and unloading behavior of minerals such as quartz, feldspar, and calcite [*Swegle*, 1990; *Grady*, 1980, *Grady et al.*, 1975].

Although several shock transit-time measurements have been made previously on tuff, wave profile measurements have been employed only recently by Sandia National Laboratories [*Furnish*, 1990, 1992, 1993] and in this study. The target

Paper number 94JB00726.
0148-0227/94/94JB-00726$05.00

geometry of the Sandia wave profile experiments has several advantages but does not allow the direct observation of the structure of the shock front. We have used a different and complementary specimen geometry, which has allowed the observation of shock-front structures in both dry and rehydrated tuff. These structures indicate complex dynamic phenomena are occurring on compression and are probably caused by pore crushing or weak phase transformations.

Samples

The rock samples were taken from cores drilled into the wall of the Bristol U4AV emplacement hole at NTS at several depths from 336 m to 457 m. The tuff from the two elevations we studied, 430 m and 457 m, is from the Calico and Crater Flat formations, respectively. Both are nonwelded bedded tuffs. Physical, mineralogical, and chemical property measurements of our samples are tabulated in Tables 1-3. (Characterization of the unshocked tuff specimens was performed by TerraTek, Inc., of Salt Lake City, Utah.) Note the large variation in tuff's characteristics, such as density and air void fraction, with elevation. We chose to primarily study 430-m elevation rock because it was in the vicinity of the device working-point depth (457 m). This tuff was competent and its grain size was uniformly small (~1 mm) relative to sample thickness (7 mm). This is important to ensure these tests are representative of bulk properties. One shot, however, was made with 457-m rock for comparison purposes. This rock was not preferred because it possessed an occasional large (~3 mm) grain. This grain size is substantially larger than the laser beam diameter of the VISAR (0.5 mm) and thus might disrupt the fidelity of the measured wave profile. All the tuff specimens were sectioned into disks ~7 mm thick by 39-mm diameter.

During sample preparation it is difficult to maintain samples in the same state of saturation in which they were found. For this reason our samples originally lost a portion of the water content and became semidry. In the semidry state the sample density of ~1700 kg/m^3 was intermediate between the in situ and fullydry densities of 1910 and 1500 kg/m^3, respectively. Rehydrated samples were obtained by soaking the machined semidry samples in water and had a density 97% of the in situ value. Actual sample densities for particular shots are listed in Tables 4 and 5.

Experimental Technique

Forward Design

The target design is shown in Figure 1. This design is called a "forward" design because the tuff is in the target. The shock is generated by impact and is incident from below in Figure 1. The diagnostic probe is a laser beam incident from above. The recording system is turned on at the appropriate time by trigger pins. The rock sample is protected from desiccation by sealing it between a Cu baseplate and a Mg backplate. A LiF window in contact with the Mg backplate provides optical access for the VISAR laser beam [*Hemsing*, 1979], while avoiding a free surface which would perturb the shock propagation more than does use of the LiF window. The Mg backplate has a shock impedance similar to tuff and to the LiF window to minimize shock reflections at the interfaces. The impactor and baseplate are made of copper, since it is a dense material with well-understood shock properties. The Delron ring at the perimeter of the sample also has a shock impedance similar to tuff and prevents a shock in the aluminum outer ring from outrunning the shock in the sample. The aspect ratio (diameter/thickness) of the sample is great enough (5.5:1) to ensure that the peripheral release waves approaching the center from the side will not interfere with the VISAR measurement at the center of the Mg/LiF interface. Eight electrical shorting pins on a diameter of 42 mm around the sample perimeter provide triggering of the diagnostic system and provide shock arrival times for the shock at the first, or front, surface of the tuff. Averaging the pin arrival times yields the start time of the shock at the center of the sample face independent of projectile tilt. Since the spot size of the VISAR beam on the Mg/LiF interface is small (~0.5 mm) and centered on the second or rear sample face, the VISAR measurement is insensitive to projectile

Table 1. Physical Property Measurements of Tuff Versus Elevation

Depth, m	Density, (kg/m^3)			Water by weight, %	Porosity,%	Saturation, %	Calculated Air Voids, %
	As-Received	Dry	Grain				
336	2287	2128	*	*	*	*	*
373	1606	1277	2414	20.5	47.1	70.0	14.1
373	1660	1323	2389	20.3	44.6	75.7	10.8
384	1758	1364	2406	22.4	43.3	91.2	3.8
384	1782	1415	2403	20.6	41.1	89.4	4.4
417	1660	1279	2365	22.9	45.9	83.2	7.7
417	1668	1275	2367	23.8	46.3	85.9	6.5
430	1884	1564	2381	17.0	34.3	93.4	2.2
437	1566	1191	2358	23.9	49.5	75.9	11.9
437	1601	1221	2369	23.7	48.5	78.5	10.4
440	1889	1552	2534	17.8	38.7	87.3	4.9
440	1923	1600	2504	16.8	36.1	89.6	3.8
457	1898	1589	2305	16.3	31.1	99.5	0.5
457	1898	1589	2305	16.3	31.1	99.5	0.5

For densities of particular samples incorporated into targets, refer to Tables 4 and 5.
* Grain density measurement compromised during testing by loss of material.

Table 2. Major Oxides of 430-m Tuff

Oxide	Percentage
SiO_2	75.29
Al_2O_3	13.10
K_2O	4.74
Na_2O	3.42
Fe_2O_3	1.45
CaO	1.43
MgO	0.27
TiO_2	0.14
MnO	0.076
BaO	0.039
PO_4	0.038

tilt. Projectile bowing at these velocities is negligible. A separate calibration experiment established the time difference between the electrical and optical signal paths.

Figure 2 is a calculated distance-time plot of the important wave paths. The principal shock generated by impact of the Cu flyer at the zero of time and distance travels forward through the baseplate, rock, Mg backplate, and into the LiF window, where it is observed. Simultaneously, another shock travels backward through the Cu impactor, reflects from the rear of the Cu impactor, and travels forward as a pressure-release or rarefaction wave. The arrival time of this release wave at the laser beam provides the sound speed in the compressed rock. The shape of the release wave is important in order to know how the shock attenuates with distance and for comparison to theory.

Two independent measurements of the Hugoniot of tuff are available from the measured wave profiles: from the arrival times front and rear in the tuff, and from the amplitude of the shock. In the arrival-time method the shock transit time across the Mg is corrected for in a self-consistent manner. The arrival time method is preferred for several reasons. First, the arrival times are easily measured accurately to 1 ns by common recording electronics (1 ns is 0.05% of the transit time), whereas VISAR amplitudes are subject to an overall ~1% calibration uncertainty. Second, the shock properties of Mg and LiF need not be known accurately to deduce the shock transit time in the tuff. Third, the shock arrival time is inherently an average over all the grains, whereas the amplitude measurement might be disproportionately affected by a few large grains. In contrast, in the amplitude method the shock properties of LiF and Mg must be known accurately, since the amplitude of the shock changes upon reflection from the various interfaces.

The Hugoniot of tuff is determined from the measured impactor velocity U_i and its known Hugoniot using the method of shock impedance matching [*Zel'dovich and Raizer*, 1967] illustrated in Figure 3. The shock speed in the tuff (U_s) is determined from the total transit time minus the calculated transit time across the Mg layer. Since the Mg layer is thin (1 mm) and its Hugoniot is known, the latter calculation contributes little error. The thin solid curve in Figure 3 is the known Hugoniot of copper [*Marsh*, 1980] plotted as pressure P versus mass velocity U_p, The thick solid curve is the Cu release curve. It is an accurate assumption for a metal that its release curve is a reflection of its Hugoniot offset from the origin by the impactor velocity. The shock pressure of the tuff is described by $P=U_s\rho_0U_p$, where ρ_0 is the initial density. The latter expression is one of the Rankine-Hugoniot relations [*Mitchell and Nellis*, 1981] derived from the conservation of mass, momentum and energy across the shock front. Thus the slope ($U_s\rho_0$) of the solid line OA is determined experimentally by measured quantities, and its intersection with the Cu Hugoniot determines a single point A on the Hugoniot of tuff. Repeated experiments with different impactor velocities map out the tuff Hugoniot (dashed curve). The Rankine-Hugoniot relations can be used to reexpress the Hugoniot data in U_s-U_p or P-V spaces, where V is volume. Measurement errors in U_s, U_i and the Cu Hugoniot are <1% and cause <1% errors in U_p.

Table 3. X Ray Diffraction Data of 430-m Tuff

Mineralogy	Weight %
Clinoptilolite	73
Potassium feldspar	14
Plagioclase	9
Smeotite	2
Quartz	2
Opal-CT	2

Component weight fraction rounded to nearest percent.

If a pore-crushing process is occurring, a shoulder is expected to be observed in the leading edge of the wave profile, the thickness of which depends on pore size; for a constant pore size the width of the shoulder is not expected to grow as the shock propagates. If, however, a phase transformation is occurring, then the width of the shoulder is expected to grow because the transition causes the shock to split into two shock fronts having different speeds. The analysis is similar to the impedance matching method described above, but involves computation of an intermediate shock state.

Forward Versus Reverse Geometry Designs

Previously, the reverse target geometry [*Furnish*, 1993] was used to study shock wave profiles of tuff. In this geometry, shown in Figure 4, the rock sample is enclosed in the Al impactor, rather than in the target, as in the forward geometry case. The foam in Figure 4 is used to obtain a substantial release wave from the rear of the rock while holding the rock in place during acceleration in the impactor. The VISAR measures the collision of the Al/rock impactor against the Al/LiF target. The calculated wave paths in this case are shown in Figure 5. In the reverse geometry the structure of the shock wave front ε propagating through the rock cannot be observed, since structure only develops as the shock moves toward the sample rear, which is inaccessible to the VISAR beam. Similarly, the speed of the principal shock in the tuff cannot be directly measured. Rather, the Hugoniot point of the rock is determined from the average amplitude of the profile after the rarefaction wave β arrives at the LiF window.

In the work reported here a forward target geometry was used. Since the shape of the rise and the arrival times of the principal shock are measured directly, this geometry is more analogous to the measurement of wave fronts generated by underground explosions. Phase transitions, pore crushing, and/or other unusual compressive behaviors develop during transit and manifest themselves in the detailed shape of the shock front. Also, in the forward geometry the Hugoniot can be determined accurately from precise measurements of shock arrival times. In addition, for a given sample diameter the sample can be about

Table 4. Shock Analysis Results for Rehydrated Tuff

Shot	Impactor Velocity (km/s)	ρ_0 (kg/m^3)	U_p(km/s)	U_s (km/s)	P (GPa)
R_h	1.390	1851	1.174 ±0.2%	3.78 ±0.6%	8.19
R_i	2.323	1854	1.915 ±0.2%	4.69 ±0.7%	16.5
R_j	3.185	1852	2.57 ±0.2%	5.55 ±0.6%	26.5
R_{yz}	5.269	1903	4.08 ±0.6%	7.85 ±0.8%	61.0
R_{wx}	7.435	1903	5.63 ±0.6%	9.97 ±0.8%	106.8

U_s and U_p are analyzed shock and mass velocities in 430-m rock sample. P is the shock pressure and ρ_0 is initial density.

twice as thick in the forward geometry as in the reverse geometry before rarefaction waves from the side interfere with the VISAR measurement at the center. This increased thickness allows one to average over more grains.

A disadvantage of the forward geometry is that propagation of the rarefaction wave through the sample can be complicated by shock reflections from the LiF/Mg interface. The Mg backplate has a density (1778 kg/m^3) similar to the rock, so the reflection from the rock/Mg interface is minimal. However, the reflected wave from the LiF/Mg interface is typically 50% over the principal shock pressure in the rock. The influence of this reflection can be minimized by choosing the thicknesses of the Mg, rock, and Cu layers so that the shock reflection from the LiF does not enter the rock until after the rarefaction wave has fully transited the rock sample. This is the case depicted in Figure 2.

Results

U_s-U_p Results

The U_s-U_p data analyzed from arrival time measurements are shown in Figure 6 and tabulated in Tables 4 and 5. The Hugoniot of the wet (rehydrated) tuff lies above that of the semidry tuff. Ultrasonic measurements of the bulk sound velocity, indicated at U_p=0, also show an increase in sound velocity due to the rehydration of the rock. For the rehydrated rock the best fit line (dashed) over the entire range $0<U_p<5.6$ km/s is $U_s=2.00+1.42U_p$; for the smaller range $0<U_p<2.6$ km/s the best fit line (solid) is $U_s=2.29+1.26U_p$.

For the semidry tuff $U_s=1.70+1.28U_p$ for $0<U_p<2.3$ km/s. A single datum of 457-m elevation tuff agrees well with the rest of the 430-m data. (However, its release wave profile differs slightly.) All the data shown in Figure 6 were analyzed assuming that the shoulders in the wave profiles during compression were caused by a pore-crushing process, not a phase transition.

For the semidry tuff, the highest U_p datum (shot R_c) has U_s lying slightly below the best fit line. In other materials, a depressed U_s is often associated with a region just above a phase transition. Consistent with this, the wave profile of the next lower pressure shot R_b has a shoulder which might be interpreted as a phase transition occurring at 16 GPa, rather than pore crushing. If the former were assumed in the analysis, the U_s-U_p datum for R_b shifts slightly, as illustrated by Figure 7.

In Figure 8 our wet tuff data are compared with a variety of similarly rehydrated NTS tuff measured by Sandia National Laboratories [*Furnish*, 1990, 1992, 1993]. All our tuff has been rehydrated to densities within 97% of in situ hydration, which is in the range 16-18% water by weight. There is reasonable agreement among the various data sets for $U_p > 2.0$ km/s (P>17 GPa), and the slight nonlinearity in our high-pressure data is replicated by the Sandia data. Below 2.0 km/s there is significant variation between the tuff types. This is expected, since at lower pressures, mechanical properties such as material strength and porosity are significant relative to shock compression thermal pressure.

Measured Wave Profiles

Wet rock. Measured and calculated wave profiles for three of the shots on the wet tuff are shown in Figure 9. They show the initial rise of the principal or leading shock, minor

Table 5. Shock Analysis Results for Semidry Tuff

Shot	Impactor Velocity (km/s)	ρ_0 (kg/m^3)	U_p(km/s)	U_s (km/s)	P (GPa)
R_e	1.354	1676	1.182 ±0.2%	3.18 ±0.25%	6.3
R_d	1.774	1676	1.524 ±0.25%	3.70 ±0.4%	9.4
R_b	2.722	1727	2.28 ±0.3%	4.63 ±0.5%	18.2
R_b [PhT]	2.722	1727	2.06 ±0.3%	4.62 ±0.5%	*16.4, 18.1
R_g (457 m)	2.706	1756	2.26 ±0.3%	4.58 ±0.5%	18.2
R_c	3.170	1719	2.65 ±0.3%	4.84 ±0.6%	22.0

Rock is 430-m elevation except for shot R_g, which is 457 m. It was assumed no phase transformation occurred, except for datum R_b[PhT].
*Phase transformation assumed in this case. The first pressure is the transition onset; the second is final pressure.

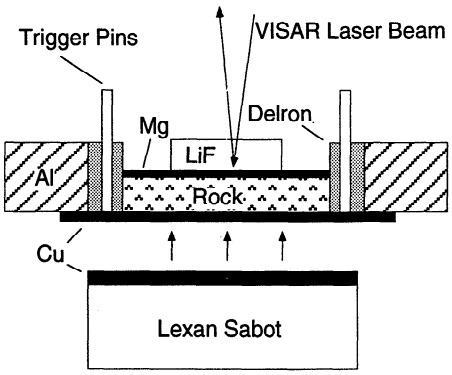

Figure 1. Target design for water-saturated rocks. Eight pins electrically detect arrival of shock. VISAR laser light reflecting off the center of LiF/Mg interface records the shock wave velocity profile.

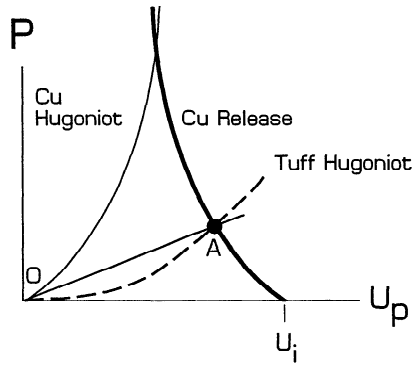

Figure 3. "Shock impedance matching" method for determining shock state of tuff (point A) from measured shock speed U_s and impactor velocity U_i. The slope of the line OA is proportional to U_s. Its intersection with the Cu release curve yields the shocked state A. The release curve is assumed to be a reflection of the Hugoniot, which for Cu is well known, offset from the origin by U_i.

reverberations, and subsequent release of pressure by the rarefaction wave as they reach the LiF window. The complex dynamics of the shock compression of tuff is manifested in the front of each of the wave profiles. For example in shot R_h the shoulder during the initial 70 ns may be due to pore crushing. This hypothesis implies an effective thickness for the shock front of $\Delta t U_s = 0.26$ mm, which is consistent with observed grain or pore size. Since the instrumental noise is small (0.5%), the observed random fluctuations are likely due to sample granularity. The feature in the wave profile at ~200 ns is probably a reflection of the principal shock from the LiF window reverberating at the Mg/LiF interface.

Semidry rock. The measured and calculated wave profiles for the semidry rock are shown in Figure 10. The lack of a plateau in the lowest pressure shots R_e and R_d is probably caused by a slower than anticipated shock speed relative to the sound speed. This allowed the rarefaction wave to overtake the shock before or as it reached the Mg/LiF interface. The lowest pressure shot R_e shows a shoulder during the initial 80 ns very similar to the lowest pressure shot R_h of the wet rock, which is probably caused by pore crushing.

The moderate pressure shot R_b also shows a shoulder, which is somewhat more pronounced. Rather than pore crushing, it is tempting to ascribe this feature to a weak phase transition, since this hypothesis also explains the depressed U_s of shot R_c relative to the best fit line. Figure 7 shows this alternative analysis. Phase transitions cause shocks within a range of pressures above an onset transition pressure to bifurcate, with the faster shock having a constant speed. The segmented solid line in Figure 7 illustrates this effect. The bifurcation generates a two-step shape in the wave profile, such as seen clearly in graphite shock transforming to diamond [*Erskine and Nellis*, 1991, 1992]. For the case here, the transition in the wave profile is very weak, corresponding to a small volume change between the two phases. The transition pressure in R_b may be just below 16.4 GPa. Shot R_g on 457-m rock does not show a shoulder, but this does not invalidate the explanation for R_b. Because of the variability of rock behavior with elevation, the transition pressure for this rock may be slightly above the

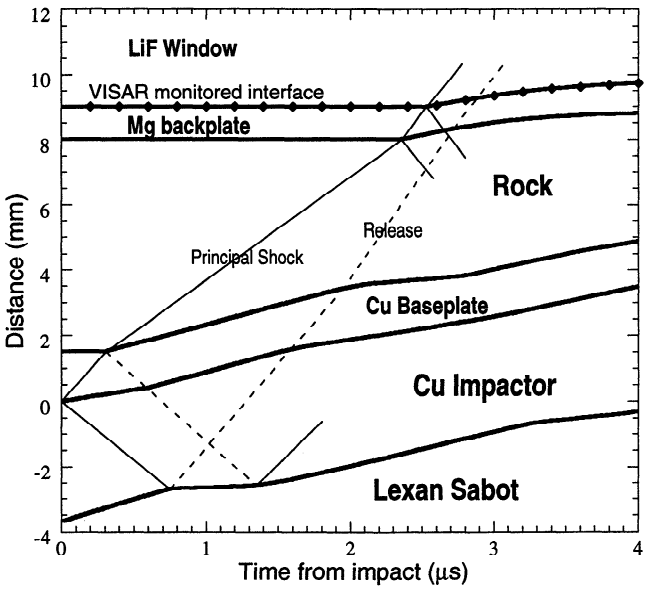

Figure 2. Wave path diagram of target/impactor collision in the forward geometry. Rarefaction waves are indicated by dashed lines, and the shocks by thin solid lines. The VISAR measures the wave profile (velocity history) at the Mg/LiF interface (diamond symbols).

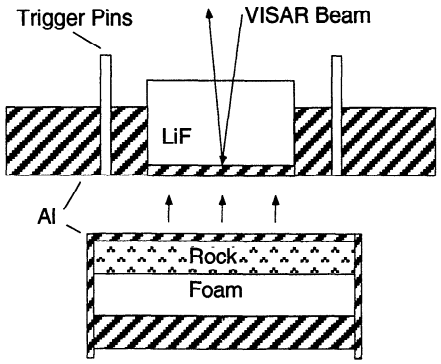

Figure 4. Experiment design for the reverse geometry after *Furnish*, 1993. The sample is enclosed by Al in the impactor. The low-density material (foam) behind the sample is used to produce a large rarefaction wave at the rear of the tuff and to support the rock during acceleration.

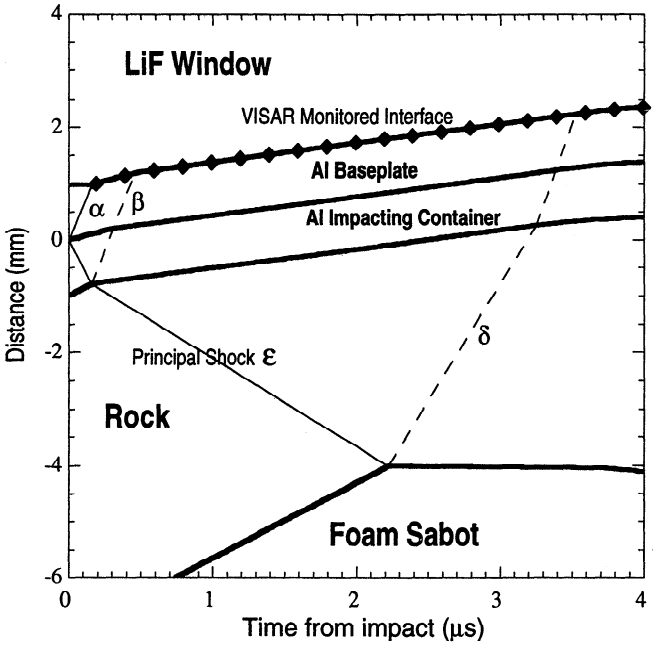

Figure 5. Wave path diagram of target/impactor collision in the reverse geometry. Rarefaction waves are indicated by dashed lines and the shocks by thin solid lines. The VISAR measures the wave profile at the Al/LiF interface (diamond symbols).

achieved pressure and so no shoulder would be produced. That the 457-m and 430-m rocks differ in some of their properties is evident by their different release behaviors in Figure 10.

For the two highest pressure shots R_{yz} and R_{wx} (not shown), because of an unexplained loss of reflected light intensity after shock arrival at the VISAR probe, the subsequent part of the measured wave profiles essentially could not be recorded. However, the shock arrival times were accurately recorded so that the U_s-U_p data from these shots are valid.

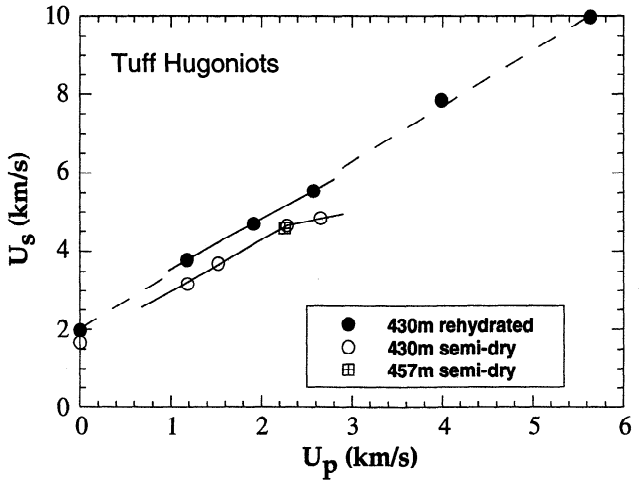

Figure 6. Hugoniot data plotted as U_s-U_p for tuff in rehydrated and semidry conditions. The data at U_p=0 are ultrasonic bulk sound speeds for 430-m rock. The semidry datum above 2.3 km/s suggests a slightly depressed U_s. Best fit lines are described in the text.

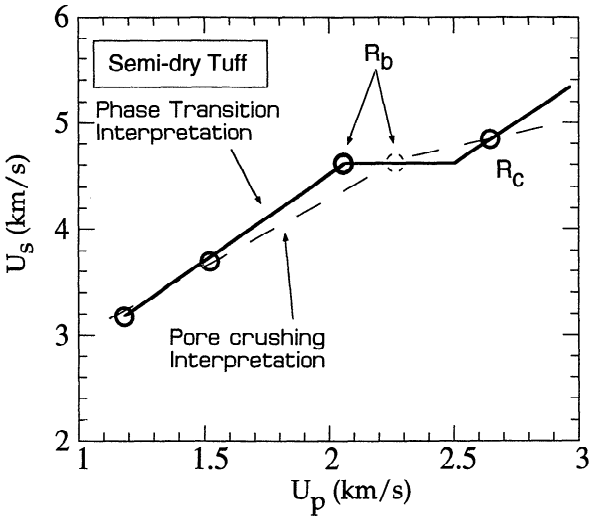

Figure 7. Alternative analysis of shot R_b. When the wave profile of R_b is analyzed interpreting the shoulder as a phase transition (solid line) instead of a pore-crushing effect (dashed line), it moves the U_s-U_p datum slightly to the left. The phase transition interpretation is relevant because it also explains the depressed U_s of the R_c datum.

Calculated Wave Profiles

The wave profiles were computed using a Gruneisen-gamma model referenced to the best fit relation of the U_s-U_p data. However, no pore crushing, phase transition or other complex behavior which could produce a shoulder were included in the model. The discrepancy between the calculated and measured curves is possibly due to this lack of complex modeling and systematic uncertainty in the VISAR amplitude calibration. The Gruneisen-gamma model is a model for uniform thermal pressure and was implemented in a one-dimensional Lagrangian hydrocode Gem [*Greenman et al.*, 1988]. In some cases, it is possible to replicate a variety of release behaviors by manipulating the model parameter γ and its volume dependence.

The Gruneisen parameter is defined by $\gamma=V(\partial P/\partial E)_V$, where V is specific volume, P is pressure, and E is specific internal energy. Parameter γ is used to describe the thermal equation of

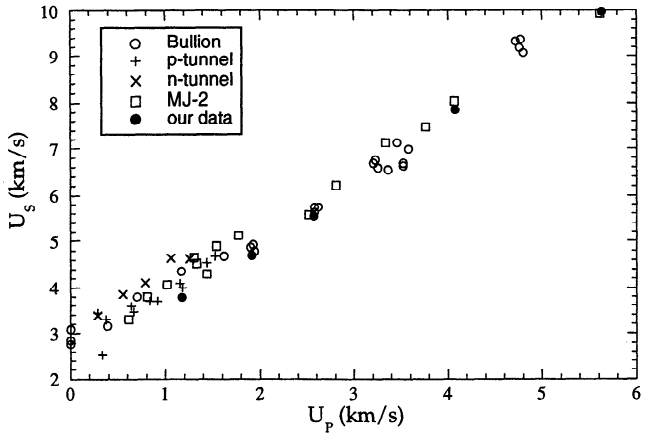

Figure 8. Our Hugoniot data compared with other data for wet tuffs from NTS measured by Sandia National Laboratories [*Furnish*, 1992]. The tuff to tuff variability is most significant at lower pressures, where mechanical effects are significant.

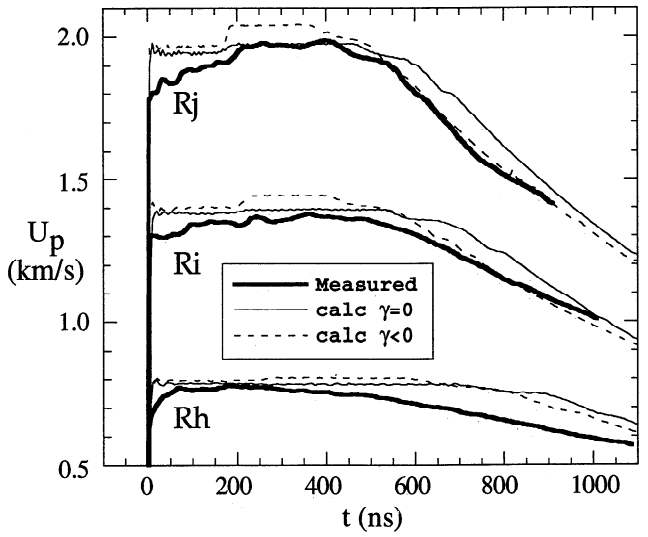

Figure 9. Measured and calculated wave profiles for wet 430-m tuff. Velocity of the Mg/LiF interface is plotted versus time. The dashed calculated curve uses gamma values from Table 6.

state near the Hugoniot curve. The states of subsequent reshocks and release are calculated [*McQueen et al.*, 1970; *Nellis et al.*, 1991] off the principal Hugoniot by including thermal pressures calculated with γ. This causes the release wave speed (sound speed) to be strongly affected by γ, with more positive γ values producing slower sound speeds [*McQueen et al.*, 1967]. Generally, for materials not undergoing phase transitions, γ lies between 0.5 and 3. Variation of γ out of this range suggests anomalous behavior. That is, for example, if γ is negative, phenomena in addition to thermal pressures are probably occurring.

In fitting release wave profiles, we found that it was not possible to reproduce the early arrival of the release wave without using negative gammas. In Figure 9, the thin line

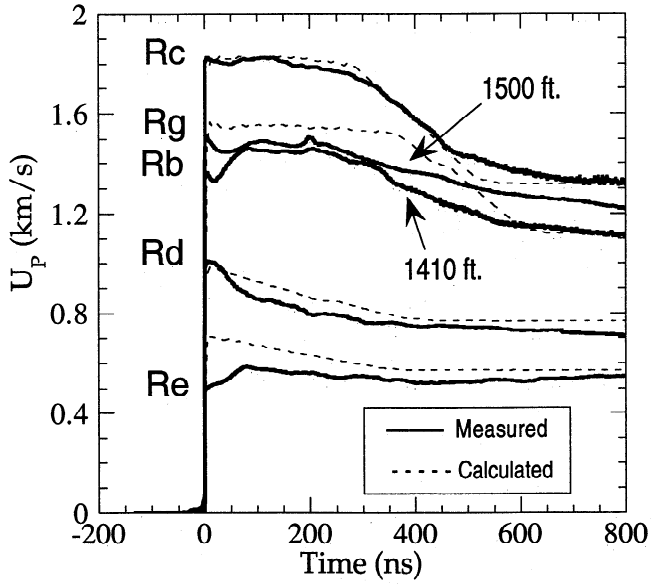

Figure 10. Measured and calculated wave profiles for the semidry rock. The rock is 430-m elevation, except for R_g, which is 457-m. One calculated curve models both R_g and R_b, since they had similar parameters.

Table 6. Gruncisen-Gamma and Its Volume Derivative Used for Calculated Wave Profiles of Wet Rock (Figure 9)

Shot Simulated	$\gamma(V_1)$	$V_0(\partial\gamma/\partial V)$	V_1/V_0
R_h	-1.75	25	0.690
R_i	-2	25	0.592
R_j	-1.5	25	0.536

V_1 and V_0 are the shock and ambient volumes.

curves were calculated with γ=0. The dashed curves, which have better agreement with the release portion of the curves, use negative gamma values listed in Table 6. The calculated curves in Figure 10 use the gamma values in Table 7.

The impedance matching analysis produces predictions for the amplitude of the wave profiles which are nearly identical to the initial amplitude of the wave profiles calculated with the hydrocode. This is because the front of the calculated curve does not depend on γ, is based on the best fit U_s-U_p relation, and the best fit line of U_s-U_p agrees with the data.

Sound Speeds

Figure 11 shows sound speeds (Eulerian) in the frame of stationary compressed tuff determined from the transit time of the rarefaction wave. This wave originates at the rear of the Cu impactor and travels forward through the Cu impactor, baseplate, and tuff (dashed line in Figure 2). The portion of the propagation time of the rarefaction wave through the copper and the Mg were calculated by one-dimensional hydrocode [*Greenman et al.*, 1988]. The mass velocity and compressed thickness of the sample were accounted for by using the measured tuff Hugoniot. The dominant uncertainty is in identifying the beginning of the rarefaction wave in the measured wave profile. For shot R_d, it appears that the release wave overtook the principal shock before reaching the LiF window, implying a sound speed of at least 6 km/s at 9.4 GPa. Also shown are sound speeds in two wet NTS tuffs measured by Sandia [*Furnish*, 1990] at lower pressures. They show an initial increase in sound speed with pressure that levels out at 10 GPa, consistent with our data.

Discussion

Tuff is a brittle porous fine-grained multiphase siliceous rock. High shock pressures cause macroscopic volume change by the compression of minerals and by pore collapse. In addition, pores are heated locally and heterogeneously under shock, which can cause nucleation of chemical reactions and/or

Table 7. Gruneisen-Gamma and Its Volume Derivative Used for Calculated Wave Profiles of Semidry Rock (Figure 10)

Shot Simulated	$\gamma(V_1)$	$V_0(\partial\gamma/\partial V)$	V_1/V_0
R_e	-2	25	0.628
R_d	-2	25	0.588
R_b, R_g	-3	0	0.543
R_c	-3	0	0.453

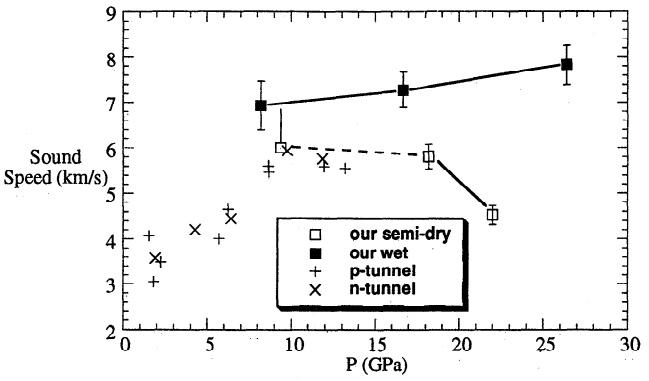

Figure 11. Measured Eulerian sound speeds in shocked 430-m tuff (wet and semidry) compared with two other wet tuffs (n, p tunnels) also from NTS [*Furnish*, 1990]. Error bars reflect uncertainty in defining arrival time of release wave. The semidry datum at 9.4 GPa is 6 km/s or greater.

phase transitions. This behavior is expected to depend on water content and is probably irreversible in general. These phenomena can affect both the compressive and release behaviors in ways which are difficult to predict in this complex heterogeneous material. The measured shock wave profiles indicate how tuff behaves at dynamic high pressure and might provide insight as to which of these various phenomena affect the wave profiles.

Compression

We have found clear experimental evidence in tuff for complex behavior in compression, which is manifested by shoulders in the leading edge of the wave profiles. The present data, however, cannot in themselves identify the source of this behavior. It is likely that the shoulders are caused by a combination of pore crushing and phase transitions which could vary in degree with hydration and pressure. The phase transition hypothesis is attractive in the semidry tuff case, since it explains the observed depression of U_s and the decrease of sound speed above the proposed transition pressure of 16 GPa. However, in the wet tuff such a depression in U_s does not occur. In this case, the shoulders are probably caused by pore crushing and the heterogeneous heating at pores is expected to be reduced with respect to the semidry samples. The data show that the shoulders are observed inconsistently in the dry tuff but relatively consistently in the wet tuff. This would suggest that water-filled pores give a more regular risetime in the wave profile than a distribution of empty pores. An experimental test of the importance of pores on loading would be to perform wave profile measurements on samples having several times greater thickness. This would determine whether the shoulder width is independent of propagation distance, consistent with pore crushing, or whether the initial width grows linearly with distance, consistent with a bifurcating wave of a phase or elastic-plastic transition.

Experiments with thicker samples are also important for defining the relevance of laboratory data to field application. It has been assumed that the shock behavior over several mm can be extrapolated to several meters. In light of shoulders in the shock front that have developed to 5% in amplitude over several mm, it would be useful to know how these shoulders vary over substantially larger propagation distances.

Release

Since the release behavior of most materials can be adequately described by a Gruneisen-gamma model using positive gammas, it is anomalous that negative gammas are required with tuff. Even with negative gammas, the release wave shape is not reproduced accurately for the lowest pressure shot (8 GPa) in wet tuff R_h. Our wave profiles do not indicate a two-wave structure on release, and so strong strength affects are not apparent.

The Gruneisen-gamma model is a single-phase thermal model which by definition is not expected to replicate complex compressive behavior. A multiphase equation of state model is needed to study the shock physics of tuff. A starting point would be the mixed-phase EOS model that *Swegle* [1990] used to model shocked quartz. In quartz he observed a phase transition from quartz to a high-pressure phase assumed to be stishovite, which is sluggish, and anomalous irreversible release behavior. Using the mixed-phase model, he was able to separate material strength effects from hysteretic effects due to reverse phase-transition kinetics. This approach illustrates the complex nature of release in pure dense SiO_2; the nature of release and reversibility in heterogeneous tuff is much more complex.

However, if one is willing to ignore the complex compressive behavior of tuff, it is possible to model the anomalous release behavior using a single-phase Gruneisen-gamma model. *Sinz et al.* [1993] have successfully replicated Sandia's release wave profiles for tuff using a Gruneisen EOS that includes a pressure dependent strength and a positive gamma. To replicate the high release wave speed, they postulate a shear modulus and yield strength that grows extremely large to 60 GPa and 1.8 GPa, respectively, at 27 GPa. We find these values surprisingly high, in light of wave profile experiments showing quartz, feldspar and calcite to exhibit fluidlike response upon release [*Grady*, 1980]. Shock recovery experiments on these minerals show mixed amorphous and crystalline phases [*Ashworth and Schneider*, 1985; *Gratz et al.*, 1992, and references therein], consistent with a multiphase model. Shock recovery experiments on tuff could be very useful to investigate irreversibility.

Conclusions

Tuff shows anomalous behavior both in compression and release. The former has only been observed with our forward geometry wave profile technique. The origin of the complex compressive behavior could be a combination of pore crushing and phase transitions which occur in varying degrees dependent on hydration and pressure. This issue could be clarified in wave profile experiments using much thicker samples, where the evolution of the wave front shoulder could be observed.

Except for the shots above 17 GPa, the Gruneisen model did a relatively poor job of modeling the release behavior and requires negative Gruneisen-gamma values, which generally indicates a phase transition. Because of the heterogeneous distribution of water-filled pores and associated heterogeneous heating, it is quite likely that this material undergoes a phase transition at high shock pressures and that its high-pressure shock properties are fluidlike. The high-pressure properties of heterogeneous tuff suggest modeling tuff with a mixed-phase equation of state. It is also very important to determine the

nature of the irreversibility of heterogeneous tuff at high shock pressures.

The U_s-U_p relation of the shock front propagating several millimeters can be accurately measured by the present technique. However, it has not been determined to what extent the shoulders in the wave front continue to evolve over 1000-fold greater propagation distances. This could affect the applicability of the laboratory-measured Hugoniots to shock propagation over large distances from nuclear yield tests. We observe an overall increase in the shock speed when dry rock is rehydrated.

Acknowledgments. We acknowledge Lew Glenn for his support, and William Moss and John White for helpful discussions. Work was performed under the auspices of the U.S. Department of Energy by the Lawrence Livermore National Laboratory under contract W-7405-ENG-48.

References

Ashworth, J.R., and H. Schneider, Deformation and transformation in experimentally shock-loaded quartz, *Phys. Chem. Miner., 11*, 241-249, 1985.

Erskine, D.J., and W.J. Nellis, Shock-induced martensitic phase transformation of oriented graphite to diamond, *Nature, 349*, 317-319, 1991.

Erskine, D.J., and W.J. Nellis, Shock-induced martensitic transformation of highly oriented graphite to diamond, *J. Appl. Phys., 71*, 4882-4886, 1992.

Furnish, M., Measuring the dynamic compression and release behavior of the paintbrush and tunnel bed (NTS) tuffs over the range 1-13 GPa, *Sandia Natl. Lab. Tech. Rep., SAND90-1317*, 1990.

Furnish, M., Measuring the dynamic compressive and release behaviors of rocks and grouts associated with hydroplus, *Sandia Natl. Lab. Tech. Rep., SAND92-0984*, 1992.

Furnish, M., Recent advances in methods for measuring the dynamic response of geological materials to 100 GPa, *Int. J. Impact Eng., 14*, 267-277, 1993.

Glenn, L.A., Modeling the explosion-source region: An overview, Proceedings of the Numerical Modeling for Underground Nuclear Test Monitoring Symposium, edited by S.R. Taylor and J.R. Kamm, *Los Alamos Sci. Lab. Rep., LA-UR-93-3839*, 17-24, 1993.

Grady, D.E., Shock deformation of brittle solids, *J. Geophys. Res., 85*, 913-924, 1980.

Grady, D.E., W.J. Murri, and P. DeCarli, Hugoniot sound velocities and phase transformations in two silicates, *J. Geophys. Res., 80*, 4857-4861, 1975.

Gratz, A.J. , W.J. Nellis, J.M. Christie, W. Brocious, J. Swegle, and P. Cordier, Shock metamorphism of quartz with initial temperatures -170 to +1000°C, *Phys. Chem. Miner., 19*, 267-288, 1992.

Greenman, G., K. Hainebach, J.A. Leibee, C. Lund, and J. Rogers, Gem Lagrangian hydro-code, Lawrence Livermore Natl. Lab., Livermore, Calif., 1988.

Hemsing, W.F., Velocity sensing interferometer (VISAR) modification, *Rev. Sci. Instrum., 50*, 73-78, 1979.

Howard, N.W., Variation in properties of nuclear test areas and media at the Nevada test site, *Lawrence Livermore Lab. Rep., UCRL-53721*, 1985.

Marsh, S.P. (Ed.), *LASL Shock Hugoniot Data,* p. 57, University of California Press, Berkeley, 1980.

McQueen, R.G., S.P. Marsh, and J.N. Fritz, Hugoniot equation of state of twelve rocks, *J. Geophys. Res., 72*, 4999-5036, 1967.

McQueen, R.G. , S.P. Marsh, J.W. Taylor, J.N. Fritz, and W.J. Carter, The equation of state of solids from shock wave studies, in *High-Velocity Impact Phenomena*, edited by R. Kinslow, pp. 293-338, Academic Press, San Diego, Calif., 1970.

Mitchell, A.C., and W.J. Nellis, Shock compression of aluminum, copper and tantalum, *J. Appl. Phys., 52*, 3363-3374, 1981.

Nellis, W.J., H.B. Radousky, D.C. Hamilton, A.C. Mitchell, N.C. Holmes, K.B. Christianson, and M. van Thiel, Equation-of-state, shock-temperature, and electrical-conductivity data of dense fluid nitrogen in the region of the dissociative phase transition, *J. Chem. Phys., 94*, 2244-2257, 1991.

Sinz, K., and W. Moss, It's material strength, not a negative Gruneisen gamma, *Lawrence Livermore Lab. Rep., UCRL-JC-112880*, 1993.

Swegle, J.W., Irreversible phase transitions and wave propagation in silicate geologic materials, *J. Appl. Phys., 68*, 1563-1579, 1990.

Taylor, S.R., Three-dimensional crust and upper mantle structure at the Nevada test site, *J. Geophys. Res., 88*, 2220-2232, 1983.

Zel'dovich, Ya. B., and Yu. P. Raizer, *Physics of Shock Waves and High-Temperature Hydrodynamic Phenomena,* Vol. II, p. 726, Academic, San Diego, Calif., 1967.

D. J. Erskine, W. J. Nellis, and S. T. Weir, Lawrence Livermore National Laboratory, P.O. Box 808, MS L-299, Livermore, CA 94550. (e-mail: erskine1@llnl.gov)

(Received October 7, 1993; revised March 9, 1994; accepted March 15, 1994.)